MODELLING THE GROWTH OF TRIGLYCINE SULPHATE CRYSTALS IN SPACELAB 3

HAK-DO YOO* and WILLIAM R. WILCOX
Department of Chemical Engineering and Center for Advanced Materials Processing, Clarkson University, Potsdam, NY 13676, USA

RAVINDRA LAL
Department of Physics, Alabama A & M University, Normal, AL 35762, USA

JAMES D. TROLINGER
Spectron Development Laboratories, Inc., Costa Mesa, CA 92626, USA

ABSTRACT

Two triglycine sulphate crystals were grown from an aqueous solution in Spacelab 3 aboard a Space Shuttle. Using a diffusion coefficient of 2×10^{-5} cm^2/s, a computer simulation gave reasonable agreement between experimental and theoretical crystal sizes and interferometric lines in the solution near the growing crystal. This diffusion coefficient is larger than most measured values, possibly due to fluctuating accelerations on the order of 10^{-3} g (Earth's gravity). The average acceleration was estimated to be less than 10^{-6} g. At this level buoyancy-driven convection is predicted to add approximately 20% to the steady-state growth rate. Only very slight distortion of the interferometric lines was observed at the end of a 33 hour run. It is suggested that the time to reach steady state convective transport may be inversely proportional to g at low g, so that the full effect of convection was not realized in these experiments.

* Present address: Samsung Advanced Institute of Technology, Kihung-Eup, Kyungki-Do, South Korea.

1. Introduction

In May of 1985 a layer of triglycine sulphate (TGS) was grown from aqueous solutions onto two seed crystals in Spacelab 3 aboard a Space Shuttle. The objectives of the experiment were to determine how crystal growth from solution progresses in a nearly convection-free environment, the influence of low g growth on crystal properties, and the extent of buoyancy-driven convection in the small fluctuating accelerations that are present in the Shuttle.

In the absence of convection, crystal growth from solutions will rapidly become slower as the adjacent solution is depleted of solute, unless the growth temperature is lowered to compensate. However if the temperature is lowered too fast the growth rate will reach the level at which solvent inclusions are formed (1). In order to estimate the optimal temperature program prior to the Spacelab 3 mission, a one dimensional spherical computer model was developed and used with a diffusion coefficient D of 5×10^{-5} cm^2/s in the solution (2,3). Later the computations were repeated with $D = 1 \times 10^{-5}$ cm^2/s using both the spherical model and a newly developed two-dimensional cylindrical model (4). It was estimated that only about 10% of the supersaturation of the bulk solution is required to drive the interface kinetics; i.e. the growth is 90% diffusion-controlled.

Here we report on a comparison of the computations using the cylindrical model and the experiments. Estimates are made of the buoyancy-driven convection that occurred and its development with time.

2. Spacelab 3 experiments

The growth experiments were performed in the Fluid Experiment System (FES) designed and constructed by TRW Systems in Redondo Beach, California, with final debugging by NASA's Marshall Space Flight Center (MSFC) in Huntsville, Alabama. Based on the original concept of Lal, the growth cell in the FES was designed so that a seed crystal is cemented onto a controlled temperature rod (sting) (5,6). An optical system provided real time schlieren video, transmission holograms and reflection holograms of the entire interior of the cell (7,8).

Quantum Technology of Sanford, Florida provided 3.4 mm thick (001) cylindrical seeds for the two growth runs. For Cell 2 the seed was 15 mm in diameter and for Cell 3 10 mm diameter. In each cell the seed was covered by a polymer diaphragm cap to prevent the solution from contacting the seed prematurely. The cell was filled with a TGS solution of concentration equivalent to saturation at 45 C (9). During storage of the cell at room temperature TGS crystallized throughout the cell. In Spacelab 3 the cell was slowly heated to 70 C and held at that temperature for several hours to redissolve this material. A pump provided circulation. The temperature was reduced to 46.5 C for Cell 2 and 46 C for Cell 3, the circulating pump turned off, and the cap withdrawn from the seed crystal. The cap in Cell 2 had leaked and spurious crystals were seen upon cap removal. Several of these later grew around the periphery of the crystal, while one floated in the solution.

At cap withdrawal the solution temperature was above its saturation temperature so that dissolution was expected. The schlieren video confirmed

that dissolution was taking place as planned. After 30 minutes for Cell 2 and 40.8 minutes for Cell 3, the sting temperature and the cell wall temperature were slowly reduced. Dissolution continued for some time before the schlieren showed the beginning of growth. Figures 1 to 3 show the temperature vs. time data. Note that during the Cell 2 experiment the ground crew called for a temperature increase because they feared the growth rate was becoming too large.

During growth, accelerometers in FES measured accelerations as high as 0.1 of Earth's gravity (g), with average fluctuations of 10^{-3} g and a maximum in the power spectrum at 17 Hz. The average DC acceleration level was approximately 10^{-6} g.

After growth the cap was replaced over the crystal. The sting was withdrawn from the cell and excess solution blotted off with soft tissue. Later the crystal was pried from the sting, measured and photographed (Figures 4 and 5). While crystal properties will be reported in detail elsewhere (27), it is noteworthy that the boundaries between the seed crystals and the space-grown layers could not be seen using optical microscopy. (Earth-grown crystals typically form inclusions at this boundary, with dislocations emerging from the inclusions into material grown on top of them. (e.g. Ref. 10)) Presumably this is a reflection of the very slow transition from dissolution to growth that occurs under diffusion-controlled conditions. The top surface of both crystals was concave, indicating more rapid vertical growth around the periphery. Around the edge (001) and (010) facets formed. From one edge of the Cell 2 crystal a thin transparent sheet had grown over almost the entire surface. Such a feature has never been observed on Earth, possibly because such a thin sheet would be bent or broken due to gravity.

Holograms were developed and converted into views of the growth cell and interferograms of the solution, both parallel and perpendicular to the sting. Typical interferograms of Cell 3 are given in Figures 6 to 8. The interferograms from Cell 2 are badly distorted because of the perturbation of the concentration field by growth of the spurious crystals. If cylindrical symmetry is assumed the interferograms can be converted to refractive index maps (and vice versa), permitting the comparison of theory and experiment described later.

The side views of Cell 2 permitted R. Naumann at MSFC to measure the size and movement rate of the floating spurious crystal. Use of Stokes law with the viscosity of the solution and the densities of solution and crystal (9) yielded an acceleration level of 4×10^{-7} g (8). This must be regarded as a lower limit because movement of the crystal parallel to the line of view was not determined. Furthermore the solution was considered to be stationary, whereas some buoyancy-driven convection may have been present. Stokes law assumes that the solid object is spherical and that the solution is of uniform density, while the actual crystal was not spherical and the solution near the crystal had a lower density because it was depleted in solute due to growth.

3. Mathematical model

Details of the mathematical model, including all of the FORTRAN computer programs, are given in Reference (4). Figure 9 shows the geometry used for the numerical model of diffusion and heat conduction during growth. Heat and mass transfer due to buoyancy-driven convection were ignored. (The consequences of this are discussed later.)

Cylindrical symmetry was assumed. While the sting and the seed are cylindrical, the cell walls constitute a 10 X 10 X 10 cm cube. In addition a temperature sensor runs parallel to the sting and a vacuum line attaches to the sting, as can be seen in Figure 8. Nevertheless a cylindrical model is a reasonable approximation because the refractive index field in the solution is determined almost entirely by the concentration field, and this varies markedly only near the crystal.

Because the partial molar volume of TGS is different in the crystal and in the solution, the growth generates a gentle flow of solution toward the crystal. This flow carries both heat and mass. However examination of the terms in the transport differential equations revealed that this flow contributes only about 0.2% to the mass transfer rate and 0.001% to the heat transfer. Consequently these contributions were ignored. If we assume constant properties in the solution this leads to the differential equation for mass transfer:

$$D\left[\frac{1}{r}\frac{\partial}{\partial r}\left(r\frac{\partial C}{\partial r}\right)+\frac{\partial^2 C}{\partial z^2}\right] = \frac{\partial C}{\partial t} \qquad (1)$$

and for heat transfer:

$$k\left[\frac{1}{r}\frac{\partial}{\partial r}\left(r\frac{\partial T}{\partial r}\right)+\frac{\partial^2 T}{\partial z^2}\right] = \rho\, c_p \frac{\partial T}{\partial t} \qquad (2)$$

where the symbols are defined in the Table of Nomenclature. The temperatures at the wall and sting tip were taken to be prescribed functions of time (Figures 1 to 3). Heat flux balances and continuity of temperature were used at each phase boundary. The normal concentration gradient at sting, cap and wall surfaces was set equal to zero because of the absence of diffusion

through these boundaries. Along the cylindrical axis (r = 0) the radial concentration and temperature gradients were set to zero because of symmetry. L'Hopital's theorem was applied to eliminate the singularity in the convective terms at r = 0.

The heat transfer and mass transfer are independent of one another except at the surface of the crystal, where they are coupled by the relations for interface kinetics:

$$V_c = K(T_e - T_i) \tag{3}$$

and solubility:

$$C_i = 0.237 \exp(-1679/T_e) \text{mol/cm}^3 \tag{4}$$

The interface kinetics constant K was derived from the data of References (10,11), i.e. for a (001) face a growth rate of 1 mm/day for an interfacial undercooling of 1 K and 2.4 mm/day for a (010) face. Since the top face in the flight experiments was (001), K = 1mm/day.K was used for that face. For the side surface and for dissolution on the top surface equilibrium was assumed, i.e. infinite K so that $T_i = T_e$.

The relationship between the concentration gradient at the crystal surface and the growth rate were found from a material balance taking into account the Stefan or crystallization flow (12) and the absence of solvent (water) in the crystal:

$$V_c = \frac{D(\nabla C)_i}{C_c(1-C_i\bar{V})} \tag{5}$$

The crystallization flow gives rise to the term $C_i\bar{V}$, which equals the volume fraction of solute at the crystal surface (approximately 0.2 in these experiments). It is negligible only if the solubility of a salt is negligible, which is most definitely not true for TGS.

The foregoing set of equations were solved using the Multiple Alternating Direction Implicit (MADI) finite difference method (13). It is a modification of the Alternating Direction Implicit (ADI) method in which new values of concentration (or temperature) are calculated for each row by implicit methods using values in adjacent rows from the preceding time step (14). In the next time step of an ADI computation, new values in each column are calculated using values in adjacent columns from the preceding time step. In MADI the new value at a point is taken as the average of values calculated from adjacent rows and from adjacent columns. MADI allows larger time increments to be used than ADI with the same accuracy, thereby reducing the computation time required.

A time increment of 10 s was used for the temperature calculations and 20 s for the concentration calculations. For isothermal dissolution a negligible difference was found for a time step ranging from 0.5 s to 30 s for concentration computations.

Because the concentration gradient was expected to be largest near the crystal, a finer mesh was used there as shown in Figure 10. Because of the assumed axisymmetry, only one-half of the cell needed to be solved.

During growth the crystal surface moves relative to the cell, so that it is generally between mesh points. In order to track the top crystal surface

and the conditions there, the following operations were performed at each time step. First the interfacial temperature T_i was found by interpolating between temperatures at adjacent mesh points in the crystal and the solution. This left three unknowns in Equations 3, 4 and 5; C_i, V_c and T_e (assuming that the interfacial concentration gradient can readily be calculated once C_i is known). After eliminating V_c by setting Equations 3 and 5 equal to one another and substituting for C_i from Equation 4, the combination was solved for T_e by successive approximations. Knowing T_e, C_i was calculated from Equation 4 and V_c from Equation 3.

For the top surface during dissolution and for the side crystal surface during both dissolution and growth K was taken as infinite, and so $T_e = T_i$, C_i was calculated from Equation 4, and V_c from Equation 5.

In the computation of concentration and temperature fields the crystal was maintained in a cylindrical shape by determining new interfacial positions for the entire top surface using the growth rate computed for the midpoint between the center and the periphery. For the side surface the growth rate halfway down was used. This procedure amounts to ignoring the effect of the deviation from cylindrical shape on the heat and mass transfer, resulting in a slight underestimation of the growth rate at the periphery (top corner). In comparing theory and experiment the crystal shape vs. time was computed from the calculated growth rate at each mesh point.

4. Comparison of experiment and theory

Initial comparison of theory and experiment were made for Cell 3 because of the problems with the Cell 2 experiment (cap leakage during storage,

spurious crystals, and crystal sheet grown above top surface of seed). Figure 11 shows a comparison of the size of the actual crystal received on Earth with computed sizes for D = 1, 2 and 3 X 10^{-5} cm^2/s. The best fit with crystal thickness (height) was for D = 2 X 10^{-5} cm^2/s, and so this value was used for subsequent computations. Note that theory and experiment both produced a concave top surface, i.e. the growth rate was higher at the periphery. Likewise the growth on the side of the crystal was several times larger than on the center of the top face.

Figure 12 shows isoconcentration lines for Cell 3 at the end of the 40.83 minute isothermal dissolution period. The solute concentration is highest at the crystal surface. As the temperatures of the wall and the sting are slowly decreased, dissolution continues for a considerable time, albeit at a continually declining rate. Eventually growth begins and the solute concentration at the crystal surface declines. This leads to a maximum in concentration some distance away from the crystal in the solution, as shown in Figure 13. Figure 14 shows the iso-concentration lines at the end of the run. Note that there is no significant change in concentration at the cap, the cell walls or even the side of the sting. Thus the original assumption of cylindrical symmetry is reasonable.

As the temperature of the wall and the sting tip are reduced after the initial isothermal dissolution period, heat flows from the solution to these surfaces, resulting in a maximum of temperature in the center of the cell as shown in Figure 15. This maximum persists for some time after the end of ramping down the temperature, until eventually the solution is again isothermal.

Using the data of Reference (9) we computed refractive index maps from the temperature and concentration data. The variation in concentration has a much larger effect on refractive index than does the variation in temperature. Thus the refractive index lines look much like the isoconcentration lines. Figure 16 shows a refractive index map at the end of the isothermal dissolution, where only concentration varies in the cell. Figure 17 shows refractive index during the programmed cooldown period, at a time showing a maximum in concentration and temperature in the middle of the cell. For long times where the solution is again isothermal, the refractive index maps look exactly like the concentration maps.

Interferograms were calculated from the refractive index field in order to compare with those obtained from the Spacelab 3 holograms (see Figures 6 to 8). Since the laser beam came in the side of the cell parallel to the top crystal surface, it was necessary to compute the optical pathlength ℓ_λ in that direction (y) at every position using:

$$\ell_\lambda = \int n \, dy \qquad (6)$$

Bright interference lines pass through points at which the optical pathlength has changed by an integral number of wavelengths of the helium-neon laser (0.633 microns). Dark lines occur between the bright lines at half-integral wavelength changes in optical pathlength. Results are given in Figures 18 and 19 (for clarity, every other fringe is deleted in Figure 19). Comparison of the experimental results in Figure 6 with the calculated results in Figure 18 for the same time give perfect agreement in the number of fringes above the top crystal surface and the number intersecting the top crystal surface. At the time represented in Figures 7 and 19, the number of fringes along the top

surface of the crystal is the same from experiment and computation. Moving straight sideways from the top surface the number of fringes from the edge of the crystal to a point directly above the edge of the sting insulator is 48 from the computations and 46 from experiment.

Finally Figure 20 shows computed and experimental crystal shapes resulting from the Cell 2 experiment. In this case the amount of growth on the side of the crystal is about the same from experiment and computation, while the computed growth on the top face is over twice as much. In view of the crystal sheet that grew over the top surface, less growth is not surprising because the sheet would have prevented diffusion from the bulk of the solution. In addition there is considerable uncertainty in the initial position of the crystal because of the cap leakage. Because of the presence of spurious crystals during cap retraction it is probable that solution had leaked in about the time the cell was filled, causing crystals to nucleate and grow during the long storage at room temperature. The seed crystal must have grown a little thicker at the same time. During the 70 C dissolution period in Spacelab 3 both the spurious crystals and the seed crystal would have dissolved, with the total dissolution exceeding the amount that had crystallized during storage. Upon cooling to 46.5 C regrowth and possibly nucleation would have occurred.

5. Convection

While the accelerations in orbiting spacecraft are small, they are not zero, as indicated in Section 2 above. Because the density of the solution was not constant during the Spacelab 3 FES experiments, some buoyancy-driven

convection was to be expected. We need to separate the effects of acceleration into those due to fluctuations and those arising from the much smaller steady background. We first consider fluctuating effects and compare expectations with experimental results.

As we show shortly, the time constant for fluid mechanics is on the order of 1 to 100 minutes in an FES cell. Since the fluctuating components of acceleration had much shorter periods than this, one would not expect any direct evidence of convection such as rapid shifts in the schlieren pattern. Indeed rapid shifts in schlieren were not observed and observable shifts in interferograms were not detected even after 1 day of growth. (Double exposure holograms did sometimes reveal local changes in a few seconds.) It is conceivable that a fluctuating acceleration could cause minute movements of solution sufficient to influence mass transfer, which is very sensitive to convection for liquids. Evidence for this might be found in the diffusion coefficient required to bring experiment and convection-free theory into agreement. If such an effective diffusion coefficient exceeds independently measured values, we might conclude that convection affected the mass transfer.

As noted earlier, the effective diffusion coefficient found for these experiments is 2×10^{-5} cm^2/s. This value equals the average found by Reddy using a porous diaphragm technique for temperatures ranging from 25 to 45 C and concentrations up to 1.2 molar (15). However the scatter in the data was on the order of +/- 100%. Using a similar technique Kroes and Reiss obtained for very dilute solutions a value of 1.3×10^{-5} cm^2/s at 45 C (9). Using a

refractometric technique Novotny, Moravec and Solc obtained 0.7 X 10^{-5} cm^2/s for a saturated TGS solution at 45 C. While the foregoing indicates that fluctuating acceleration may increase mass transfer rates, the evidence is weak. A computer simulation would be most helpful, but a supercomputer is needed for a full three-dimensional time-dependent coupled fluid mechanics / mass transfer solution.

The steady background acceleration, on the order of 10^{-6} g, is expected to generate convection after some period of time (as discussed later). We can use existing correlations (16-21) to estimate the steady state contribution of this convection to the growth rate. (These correlations are for buoyancy-driven natural convection about spheres (16), cylinders (17, 21) and vertical flat plates (18-20) with low Grashof number.) The ratio of the contribution of convection to the growth rate to that for diffusion is given by:

$$\frac{V_{conv}}{V_{diff}} = \frac{Sh_{conv}\ \Delta C}{d(\nabla C)_i} \qquad (7)$$

where Sh_{conv} is the contribution of convection to the Sherwood number from a correlation. The concentration difference ΔC between solution at the crystal surface and far from it is taken to be 0.057 $mmol/cm^3$, the crystal diameter 1.5 cm, and the interfacial concentration gradient 0.44 $mmol/cm^4$. Using the properties given in the Table of Nomenclature for TGS solutions we calculate a value of 0.14 for the Grashof number Gr at 10^{-6} g and 650 for the Schmidt number Sc. From Equation (7) and the correlations we estimate a convective contribution to the growth rate ranging from 13 to 22% of the diffusive contribution.

The steady state fluid velocity due to convection is on the order of (22):

$$V = \nu\, Gr/d \tag{8}$$

for a Grashof number much less than unity, and

$$V = \nu Gr^{1/2}/d \tag{9}$$

for a Grashof number much greater than unity. With the values given above (Gr = 0.14) we use Equation (8) to estimate V = 4.5 cm/hr, which is sufficiently large that it should have been obvious in both the schlieren pattern and the inteferograms for Cell 3. The fact that distortion was not observed until very late in this run indicates that steady state convection was not obtained. We must ask ourselves how long it takes to reach steady state natural convection at low acceleration levels.

Three-dimensional time-dependent convection computations were carried out using the discrete element method (23). Unfortunately computer requirements were extremely heavy so only short periods of real time could be simulated. In order to isolate initial transient diffusion effects from transient convection effects, diffusion was allowed to proceed for 46 hours in the absence of convection for a concentration difference of 0.057 mmol/cc between the top crystal surface and the bulk solution. Figure 21 shows the maximum solution velocity in Cell 2 after turning on an acceleration of 10^{-4} g (Gr = 14). If the velocity continued to increase at the same rate, it would take 0.36 hours to reach the steady state velocity of 0.032 cm/s estimated from Equation (9). However in practice the rate of velocity increase with time

would diminish, so that more than 0.36 hours would be required to reach steady state. The question is, how much time would be required at 10^{-6} g? If the concentration field is not influenced by convection, which is not likely to be true for large Sc, the hydrodynamic transient time is independent of g level. However for the coupled mass transfer and fluid mechanics that occurs in natural convection, this may not be true.

In the literature we located three boundary layer theoretical treatments (good for large Gr) of transient natural convection from a vertical flat plate (24-26). All of these treatments agree on the Gr dependence of the transient time, but only one (24) examined the Sc dependence. The time required to reach steady state after turning on a temperature or concentration difference is approximately (24):

$$t = 5.24(0.95 + Sc)^{1/2}Gr^{-1/2}x^2/\nu \qquad (10)$$

from which we calculate 1.69 hours for the Cell 2 conditions examined above with an acceleration of 10^{-4} g and 16.9 hours at 10^{-6} g. However for low Gr, as we have for 10^{-6} g, it is likely that the 1/g dependence of transient time is greater than the one-half power. Since the g dependence of velocity goes from 1/2 power to 1 as Gr becomes small (Equations 8 and 9), it is likely that the same thing happens for transient time. If we assume a time dependence of 1/g, then we estimate a transient time of 169 hours to achieve steady state conditions. This is far longer than the length of the Spacelab 3 experiment! But is this reasonable?

6. Transients

In order to gain some theoretical guidance on the various transient times, we turn to the governing partial differential equations. The Navier-Stokes equation for hydrodynamics with the usual Boussinesq approximation is:

$$\frac{\partial V}{\partial t} + V \cdot \nabla V = \nu \nabla^2 V - \beta g \Delta C \tag{11}$$

The mass transfer equation with convection is:

$$\frac{\partial C}{\partial t} = D\nabla^2 C - V \cdot \nabla C \tag{12}$$

The convective heat transfer equation for low velocity flows is:

$$\rho c_p \frac{\partial T}{\partial t} = k\nabla^2 T - \rho c_p V \cdot \nabla T \tag{13}$$

We non-dimensionalize these PDE by dividing all lengths by a characteristic length L, all concentrations by a characteristic concentration difference ΔC, all temperatures by a characteristic temperature difference ΔT, all velocities by a reference velocity V_r, and all times by a reference time t_r. Thus the above equations become:

$$\frac{L^3 V_r}{\nu^2 t_r} \frac{\partial v}{\partial \tau} + \frac{L^2 V_r^2}{\nu^2} v \cdot \nabla v = \frac{L V_r}{\nu} \nabla^2 v - Gr \tag{14}$$

where $v = V/V_r$ is the dimensionless velocity. The first term in this equation is for acceleration, the second for inertia, the third for viscous effects, and the third comes from buoyancy and drives the convection. Similarly the

dimensionless mass transfer equation is:

$$\frac{L^2}{t_r D}\frac{\partial \phi}{\partial \tau} = \nabla^2\phi - \frac{V_r L}{D} v \cdot \nabla\phi \qquad (15)$$

The first term is the transient term, the second the diffusive transport term and the third the convective transport term. The dimensionless heat transfer equation is.

$$\frac{L^2 \rho c_p}{t_r k}\frac{\partial \psi}{\partial \tau} = \nabla^2\psi - \frac{V_r L \rho c_p}{k} v \cdot \nabla\psi \qquad (16)$$

All of the pre-differential expressions and all of the differentials in the above equations are dimensionless. The non-dimensionalising parameters must be chosen such that every differential in the PDEs is of order one. Thus a logical choice for L is the crystal diameter, for ΔC the difference in solution concentration between the crystal surface and the cell wall, and for ΔT the difference in temperature between the sting and the cell wall. The reference velocity is on the order of the maximum velocity in the system and the reference time is on the order of the transient time. The maximum velocity and the transient time are what we want to estimate.

If acceleration is zero, Gr = 0. Noting that viscous decay damps convection in the absence of a driving force, we set the acceleration term equal to the viscous term to obtain the following estimate for the transient time due to fluid mechanics alone:

$$(t_r)_{fluid} = L^2/\nu \qquad (17)$$

For a characteristic length of 1 cm and a kinematic viscosity of 0.013 cm^2/s, Equation 17 gives a transient time of 77 seconds.

In the absence of convection the convective transport terms in the heat and mass transfer PDEs are zero and the pre-differential expressions in them must be of order one. Thus the transient times for diffusion and conduction are:

$$(t_r)_{diff} = L^2/D \tag{18}$$

$$(t_r)_{cond} = L^2 \rho c_p / k \tag{19}$$

From these we estimate a transient diffusion time of 14 hours and a transient conduction time of 19 minutes for our experiments.

For large Gr, the viscous term in the momentum Equation 14 is negligible compared to the inertial term. Thus the pre-differential expression in the intertial term must equal the buoyancy term, from which:

$$V_r = Gr^{1/2} \nu / L \tag{20}$$

This is the same as reported in the literature (22). In the mass transfer equation 15, convective effects are fully established when the transient term is about equal to the convection term. Equating the pre-differentials and substituting equation 20 we obtain:

$$(t_r)_{comb} = \frac{L}{V_r} = \frac{L^2}{\nu\, Gr^{1/2}} \propto \frac{1}{g^{1/2}} \qquad (21)$$

which is the same functional dependence on g as reported in the literature for large Gr (24-26). (Implicit in the foregoing is the assumption that density differences arise entirely from concentration differences, which is a good approximation in crystal growth from solution.)

For small Gr, the inertial term in equation 14 is negligible compared to the viscous term. Equating the pre-differential expression in the viscous term to buoyancy we obtain:

$$V_r = Gr\ \nu/L \qquad (22)$$

which is the same as given in the literature (22). Substituting this into the mass transfer equation and equating transient and convective pre-differentials we obtain:

$$(t_r)_{comb} = \frac{L}{V_r} = \frac{L^2}{\nu Gr} \propto \frac{1}{g} \qquad (23)$$

7. Summary

Both experiments and theory indicate that the time required to reach steady state in buoyancy-driven mass transfer increases as the average acceleration level decreases. The same might be true for heat transfer controlled free convection, as is common in solidification. Thus some experiments performed in space may terminate before the convection reaches

steady state levels. Transient computer simulations are needed to confirm these predictions.

The experiments indicate that fluctuating accelerations may significantly enhance mass transport rates, even when global convection is not generated. Transient three dimensional computer simulations are needed to confirm this result.

The lack of vigorous convection in a space environment makes it easy to achieve a gentle transition from dissolution to growth so that solvent inclusions are not formed between the seed and the grown layers. Experiments on earth have shown that closure of such inclusions tends to result in dislocations which propagate through subsequently grown materials and degrade properties. It may be that this will permit us to grow crystals from solution in space superior to what is possible on earth. More flight experiments are needed to adequately test this possibility.

Acknowledgements

This research was supported by NASA Contract NAS8-32945 and by Clarkson University. The Principal Investigator for this program was Ravindra Lal and the Co-Investigator was Roger L. Kroes at NASA's Marshall Space Flight Center. The flight experiments were performed by Lodewijk van den Berg and Don Lind. We are grateful to the many dedicated persons at TRW Systems and NASA MSFC who helped with hardware development and operation, and especially Rudy Ruff for his continual assistance during the planning and execution of the flight experiment. Arsev Eraslan recommended the MADI computational technique and provided the discrete element program used to simulate three-dimensional convection.

References

(1) W.R. Wilcox, J. Crystal Growth 65 (1983) 133.

(2) L.C. Liu, W.R. Wilcox, R. Kroes and R. Lal, p. 389 in Materials Processing in the Reduced Gravity Environment of Space, ed. G. Rindone (Elsevier, 1982).

(3) L.C. Liu, M.S. Thesis, Clarkson University, 1981.

(4) H.D. Yoo, Ph.D. Thesis, Clarkson University, 1986.

(5) R.B. Lal, M.D. Aggarwal, R.L. Kroes and W.R. Wilcox, Phys. Stat. Solidi 80 (1983) 547.

(6) R.B. Lal, R.L. Kroes and W.R. Wilcox, p. 399 in Materials Processing in the Reduced Gravity Environment of Space, ed. G. Rindone (Elsevier, 1982).

(7) R.B. Owen and R.L. Kroes, Optics News 11 (1985) No. 7.

(8) R.B. Owen, R.L. Kroes and W.K. Witherow, Optics Letters 11 (1986) 407.

(9) R.L. Kroes and D. Reiss, J. Crystal Growth 69 (1984) 414.

(10) F. Moravec and J. Novotny, Kristall und Technik 7 (1972) 891.

(11) J. Novotny, F. Moravec and Z. Solc, Czech. J. Phys. B23 (1973) 261.

(12) W.R. Wilcox, J. Crystal Growth 12 (1972) 93.

(13) A.H. Eraslan, Numerical Analysis and Computer Methods, University Tennessee Space Institute (Tullahoma, 1969).

(14) D.W. Peaceman and H.H. Rachford, J. Soc. Ind. Appl. Math. 3 (1955) 28.

(15) B.S. Reddy, M.S. Thesis, Clarkson University (1984).

(16) W.G. Mathern, A.J. Madden, Jr., and E.L. Piret, Ind. Eng. Chem. 49 (1957) 961.

(17) J.J. Mahony, Proc. Roy. Soc. A238 (1956) 412.

(18) F.J. Suriano and K.T. Yang, Int. J. Heat Mass Transfer 11 (1968) 473.

(19) S.W. Churchill and H. Ozoe, Trans. ASME 95C (1973) 540.

(20) F. Geoola and A.R.H. Cornish, Int. J. Heat Mass Transfer 25 (1982) 1677.

(21) Y.T. Shee and S.N. Singh, Natural Convection, American Society of Mechanical Engineers (1981).

(22) S. Ostrach, Ann. Rev. Fluid Mech. 14 (1982) 313.

(23) A. Eraslan, W.L. Lin and R.D. Sharp, FLOWER: A computer code for simulating three-dimensional flow, temperature, and salinity conditions in rivers, estuaries and coastal regions, NUREG/CR-3172, ORNL/TM-8401, Oak Ridge National Laboratory, Oak Ridge, Tennessee (1983).

(24) R. Siegel, Trans. ASME 80 (1958) 347.

(25) R.J. Goldstein and D.G. Briggs, J. Heat Transfer 86 (1964) 490.

(26) G.D. Callahan and W.J. Marner, Int. J. Heat Mass Transfer 19 (1976) 165.

Nomenclature
(Properties used in computations are given in parentheses)

C - Concentration of TGS in solution (mol/cm^3)

ΔC - Difference in solution concentration at crystal surface and in bulk solution (mol/cm^3)

C_c - TGS concentration in crystal (ρ_c/M) (5.23×10^{-3} mol/cm^3)

C_i - Solution concentration at crystal surface

c_p - Heat capacity - of solution (5×10^3 J/kg.K)

- of crystal (1.5×10^3 J/kg.K)

- of Teflon (1.26×10^3 J/kg.K)

- of Dow Corning 732 RTV adhesive (1.46×10^3 J/kg.K)

D - TGS diffusion coefficient in solution (2×10^{-5} cm^2/s)

d - Diameter of crystal (1 and 1.5 cm)

Gr - Grashof number for mass transfer, $g_a \beta d^3 \Delta C/\nu^2$

g - Earth's gravitational acceleration (9.8 m/s^2)

g_a - Acceleration (m/s^2)

K - Interface kinetics constant (1.16×10^{-8} m/s.K for (001) TGS)

k - Thermal conductivity - of solution (0.5 J/m.k.s)

- of crystal (0.68 J/m.k.s)

- of Teflon (0.41 J/m.k.s)

- of cement (0.19 J/m.k.s)

L - Characteristic length (d or half of cell width)(m)

ℓ - Optical path length (m)

M - Molecular weight (323 g/mol for TGS)

n - Refractive index

Sc - Schmidt number of solution, ν/D (650)

r - Radial position (m)

Sh_{conv} - Sherwood number due to convective mass transfer

T - Temperature (K)

T_e - Equilibrium temperature corresponding to solubility (K)

T_i - Temperature at crystal surface (K)

ΔT - Temperature difference (K)

t - Time since retraction of cap (s)

t_r - Characteristic transient time (s)

$\bar{V}$ - Partial molar volume (181 cm^3/mol)

V - Velocity (m/s)

V_c - Crystal growth rate (m/s)

V_r - Reference velocity (m/s)

v - V/V_r, Dimensionless velocity

z - Axial position (m)

β - Concentration densification coefficient of solution, $(-\partial\rho/\partial C)_T/\rho$ (0.46 cm^3/mol)

∇ - Gradient (m^{-1})

ϕ - $(C - C_i)/\Delta C$, Dimensionless concentration

ν - Kinematic viscosity of solution (0.013 cm^2/s)

ψ - $(T - T_i)/\Delta T$, Dimensionless temperature

ρ - Density - of solution (1.16 g/cm^3)

- of crystal (1.69 g/cm^3)

- of Teflon (2.3 g/cm^3)

- of cement (1.03 g/cm^3)

τ - t/t_r, Dimensionless time

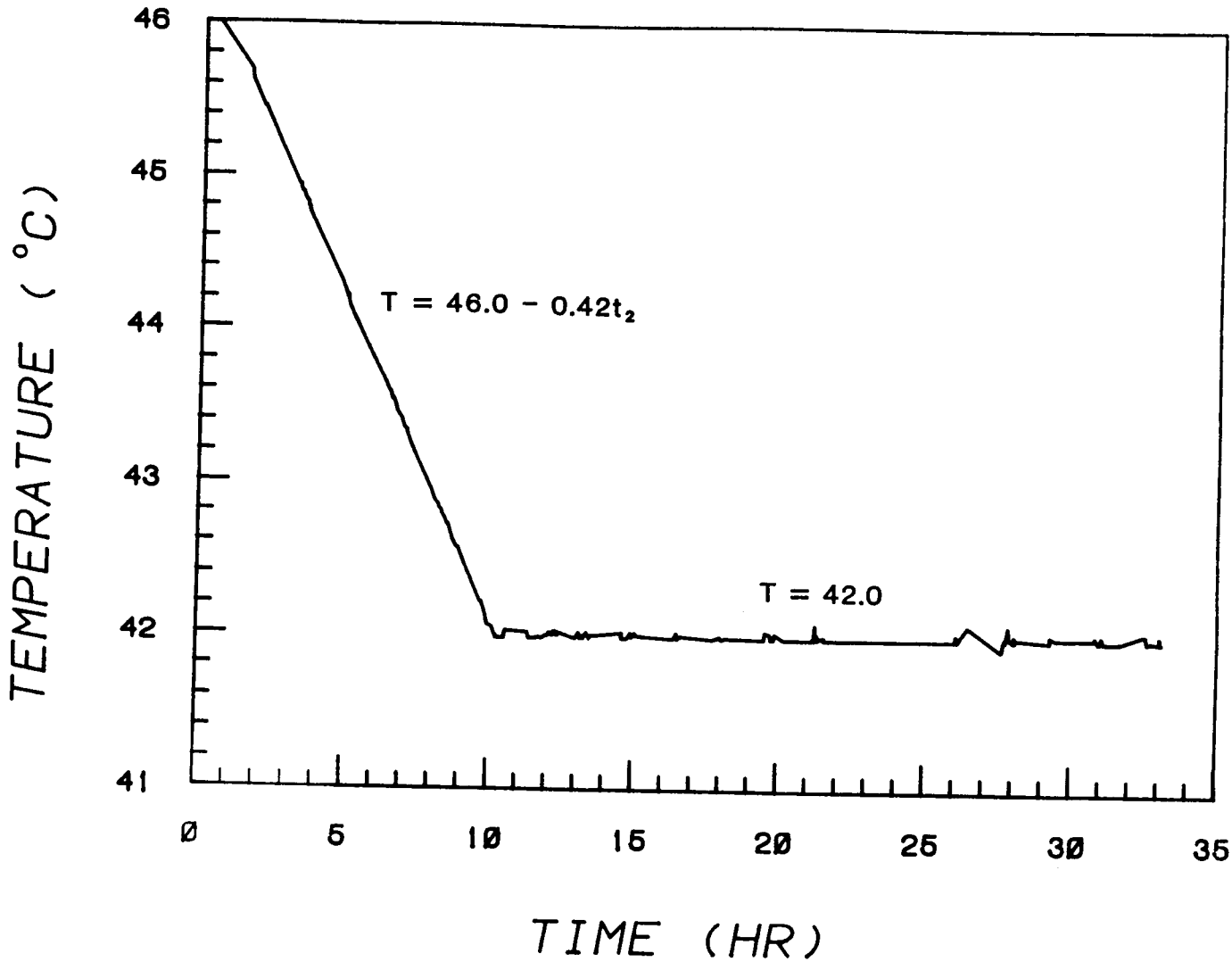

Figure 1. Measured sting temperature vs. time for Cell 3. Wall temperature the same within experimental error.

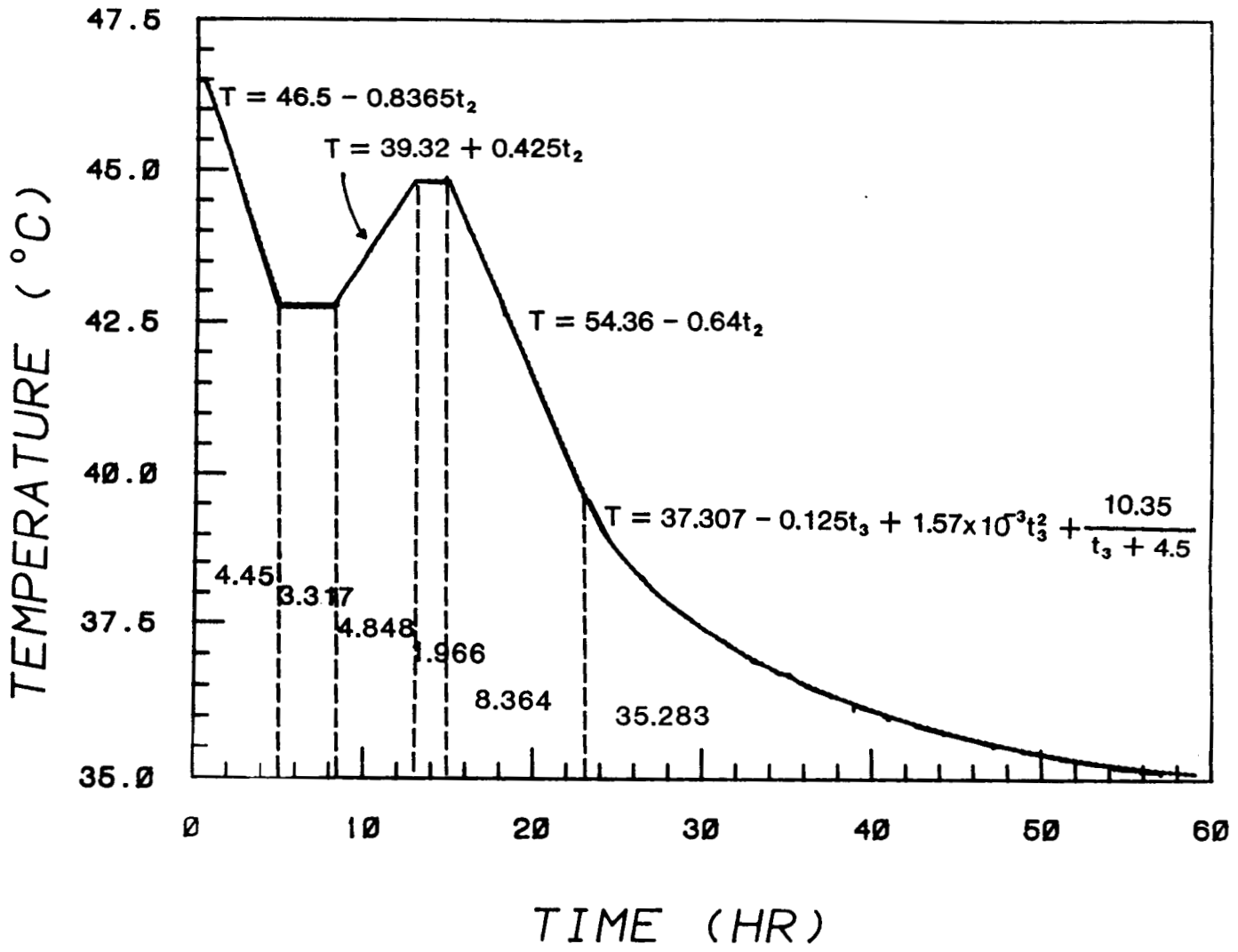

Figure 2. Measured sting temperature vs. time for Cell 2.

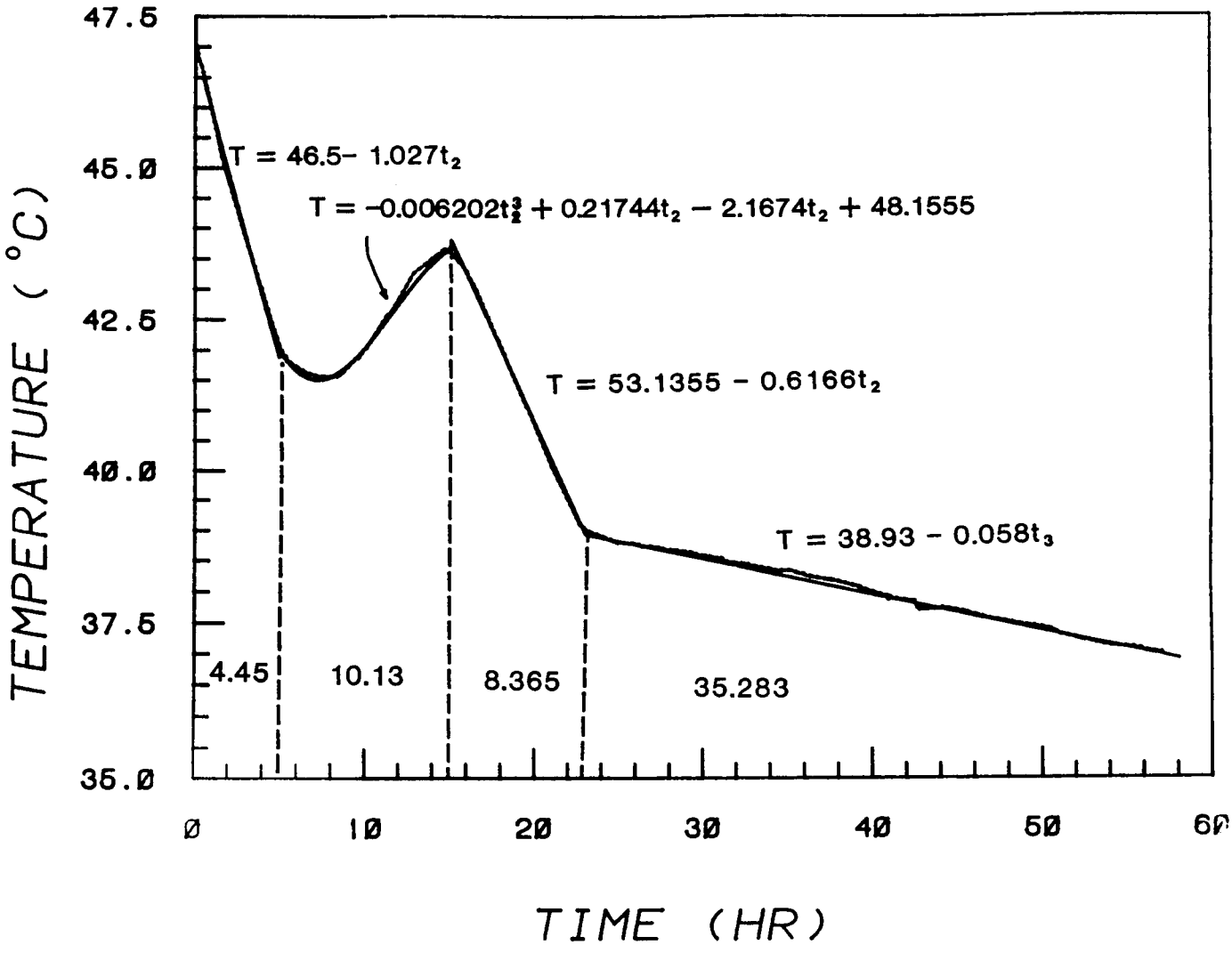

Figure 3. Measured wall temperature vs. time for Cell 2.

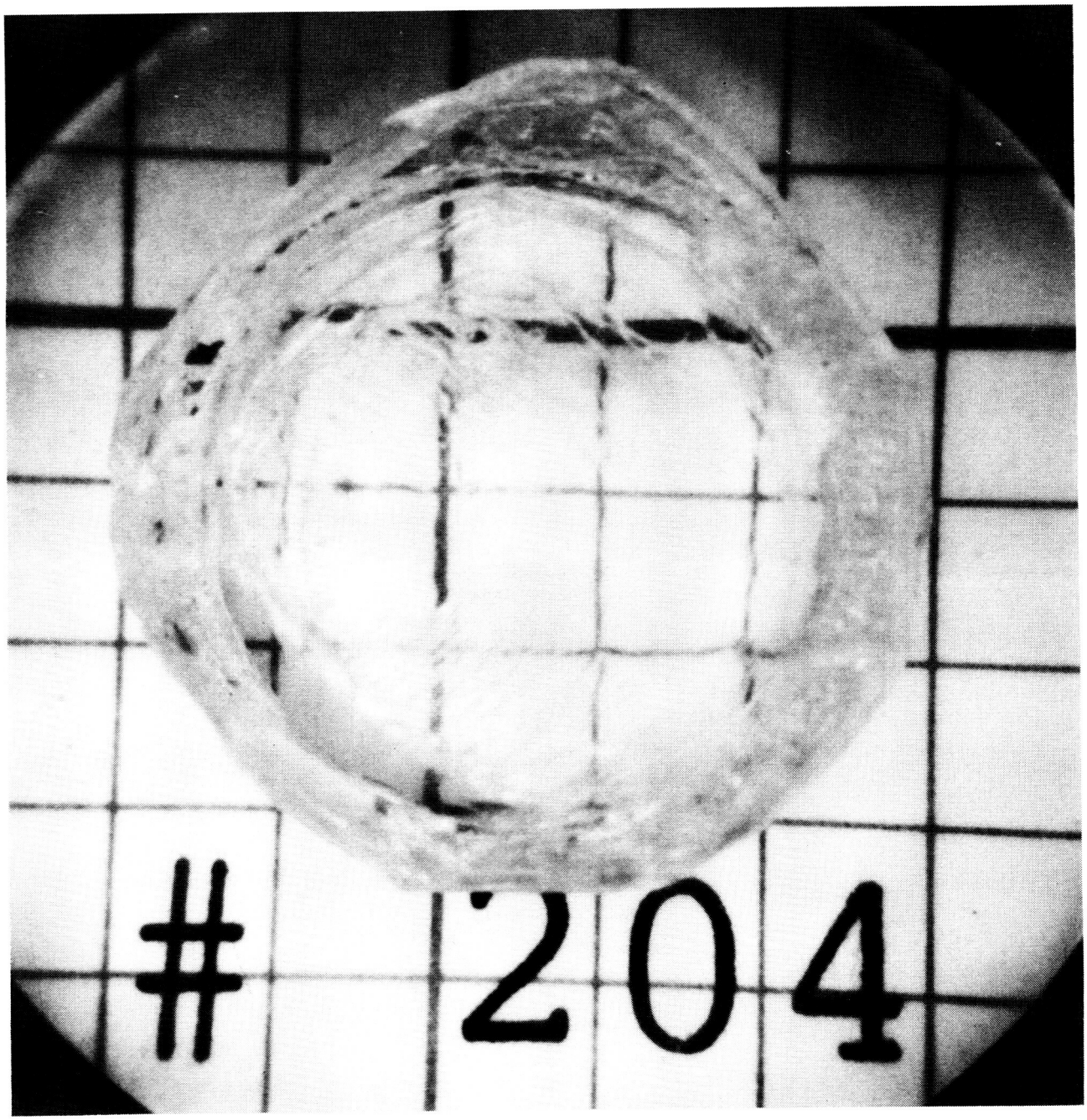

Figure 4. Top view of TGS crystal grown in Cell 3.

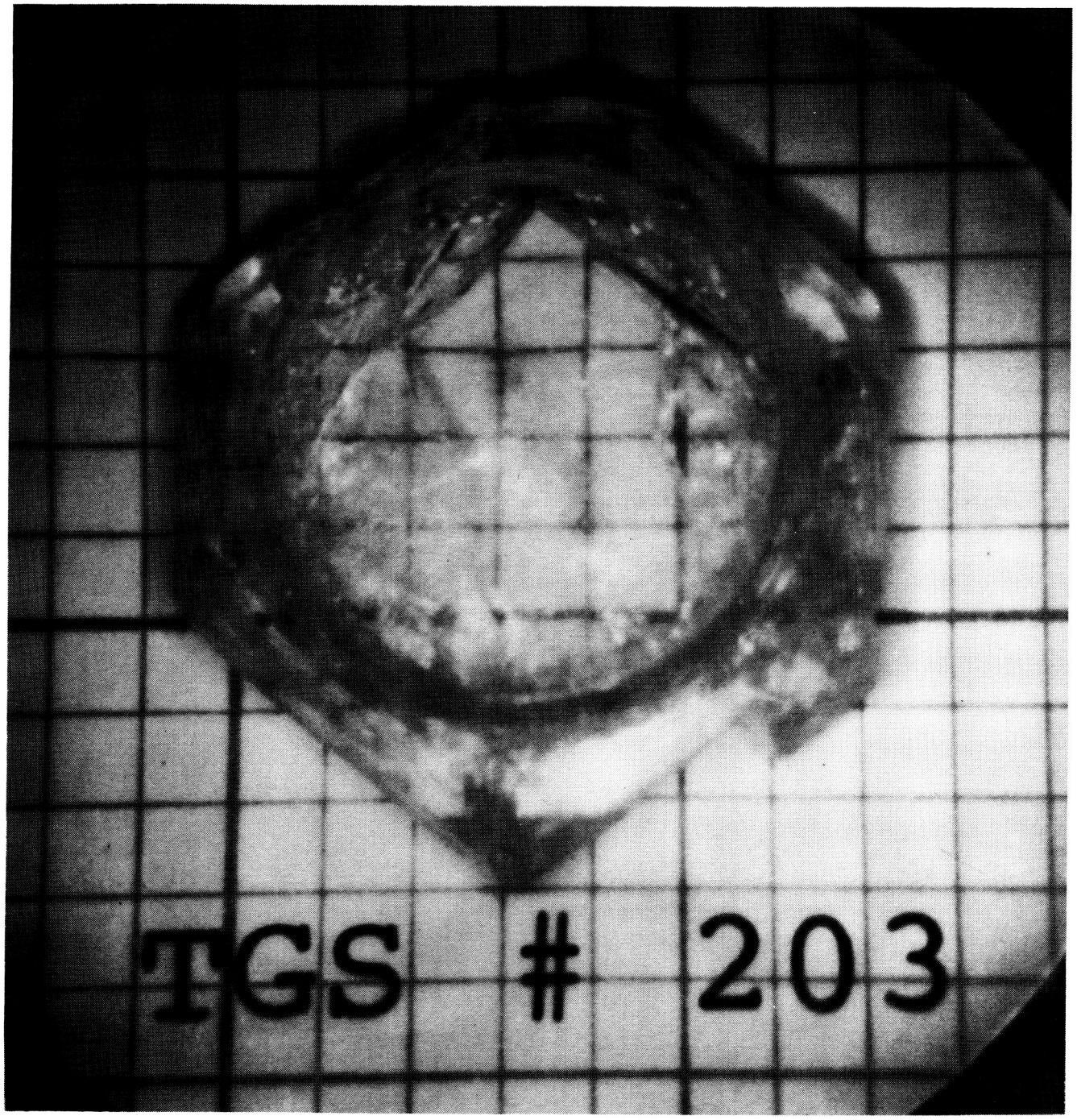

Figure 5. Top view of TGS crystal grown in Cell 2.

Figure 6. Cell 3 Holographic interferogram of solution near crystal 40.83 minutes after initiation of cap retraction. Object at bottom is mask used to cover image of sting and growing crystal to enhance quantitative comparison with theoretical predictions.

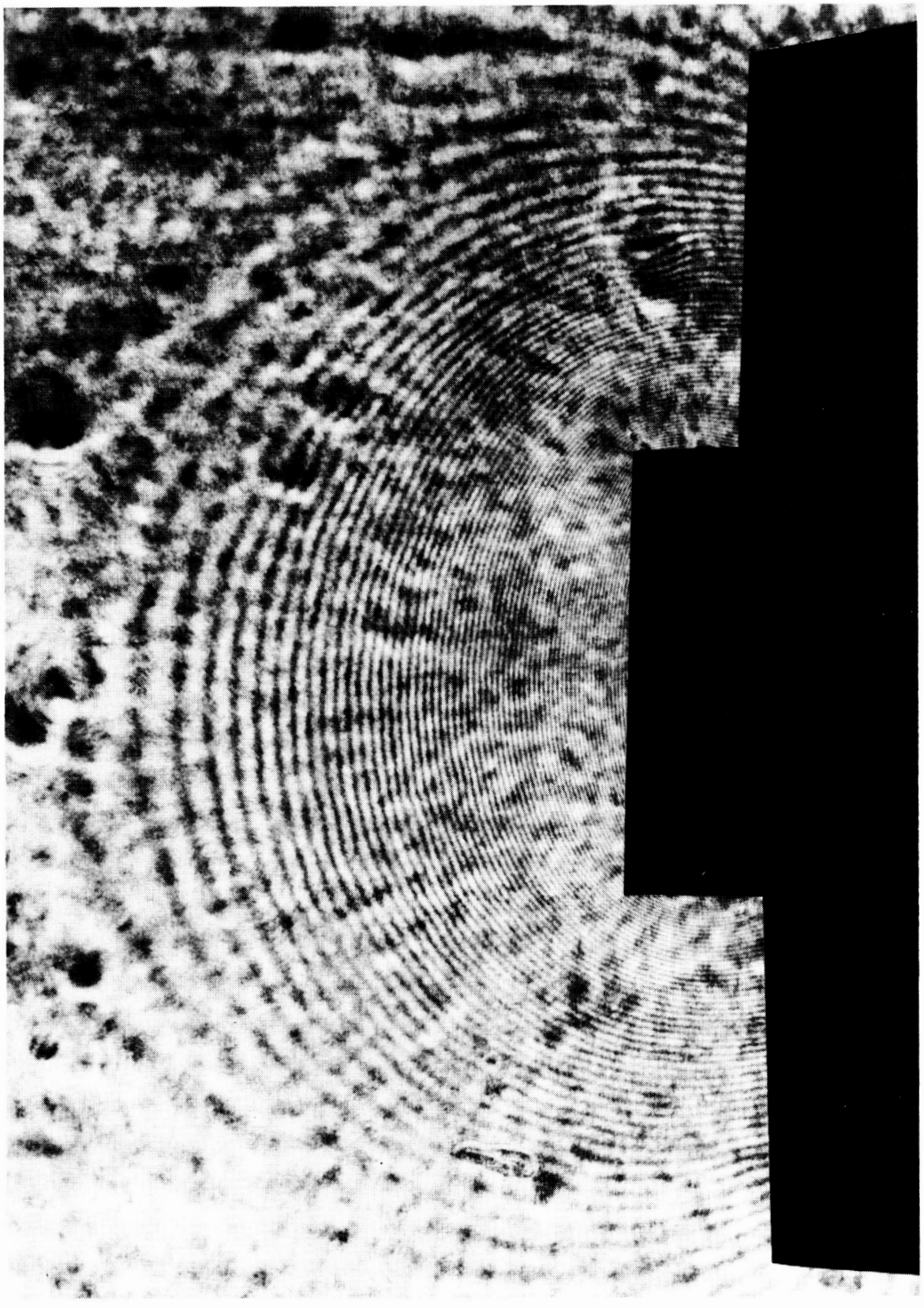

Figure 7. Cell 3 interferogram 16.87 hours after cap withdrawal.

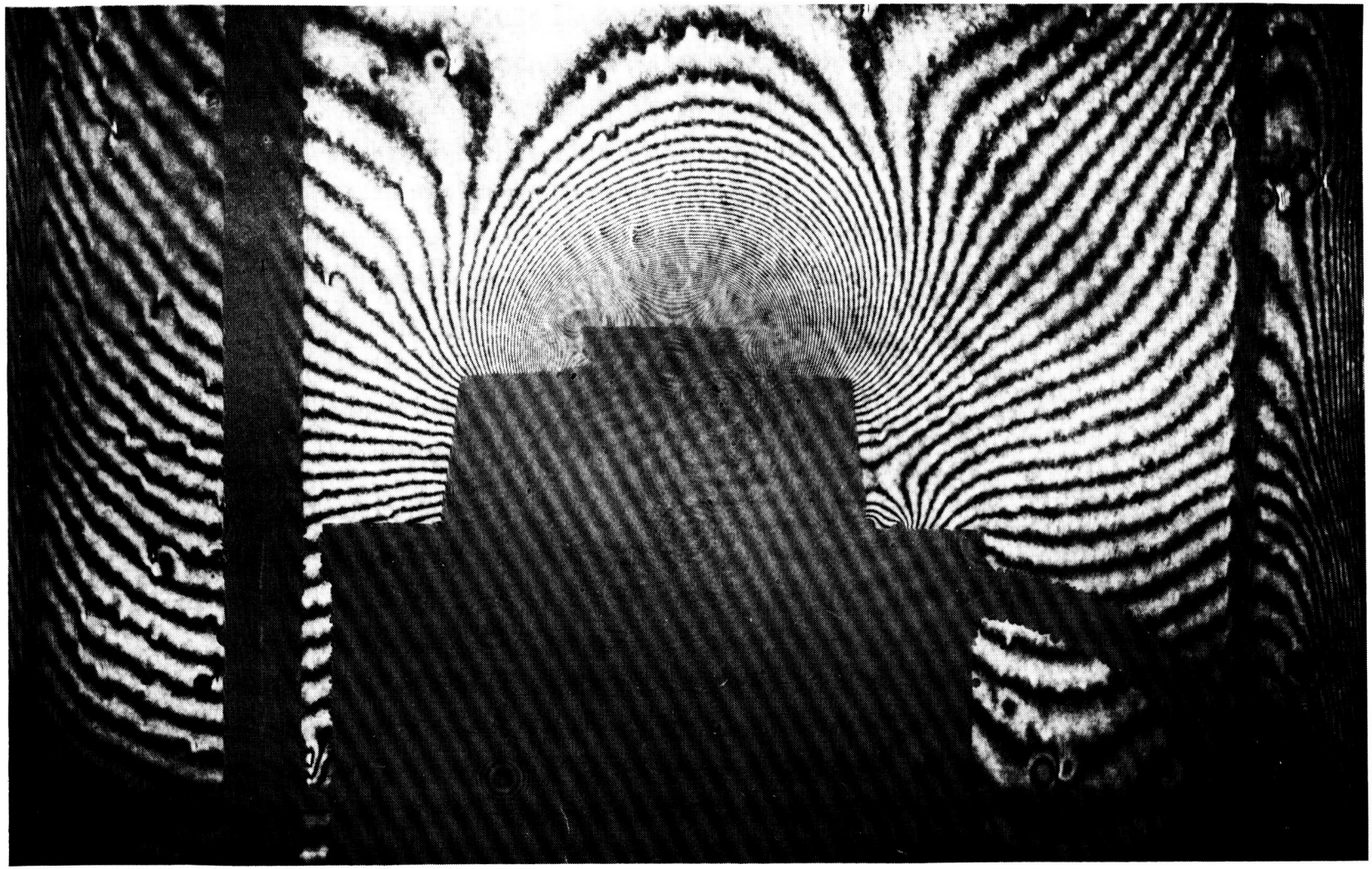

Figure 8. Cell 3 interferogram 24.33 hours after cap retraction. Actual image of sting and crystal are seen in center. Vertical rod to left of sting is thermal sensor. Rod curving down from right side of sting is vacuum line.

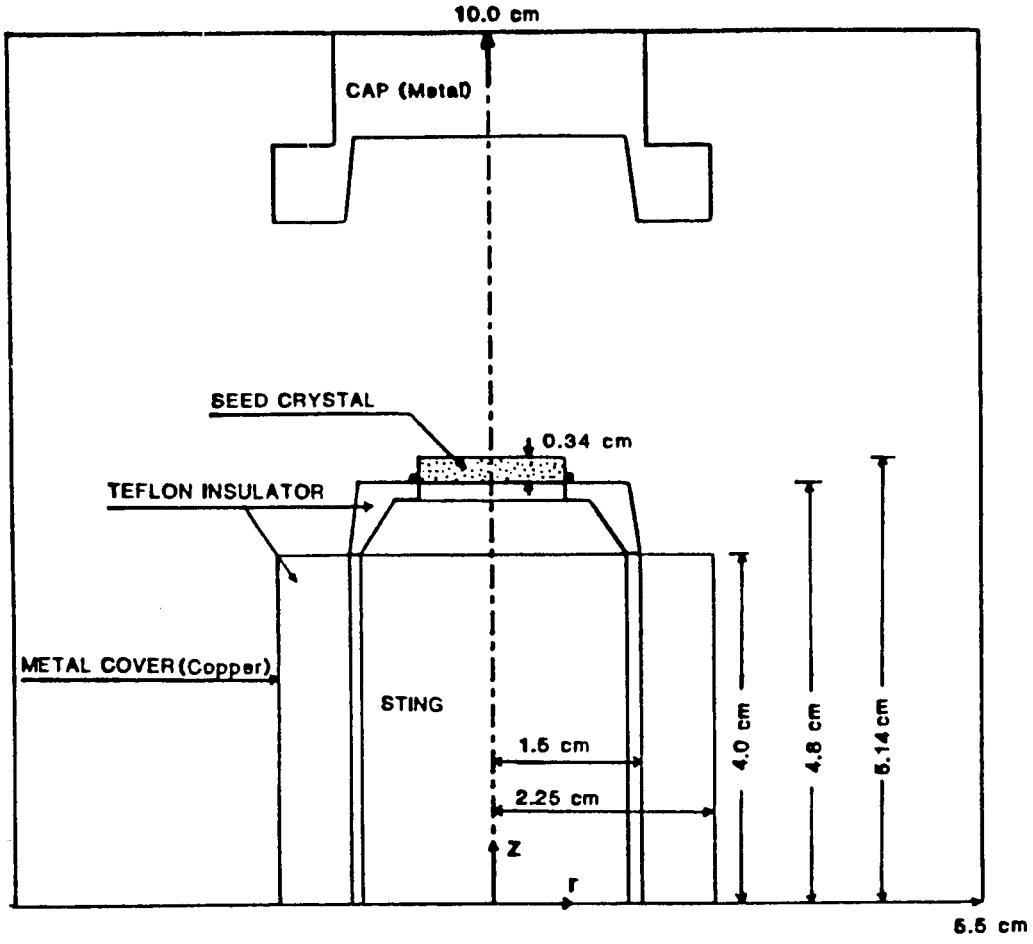

Figure 9. Cell geometry used in computer model.

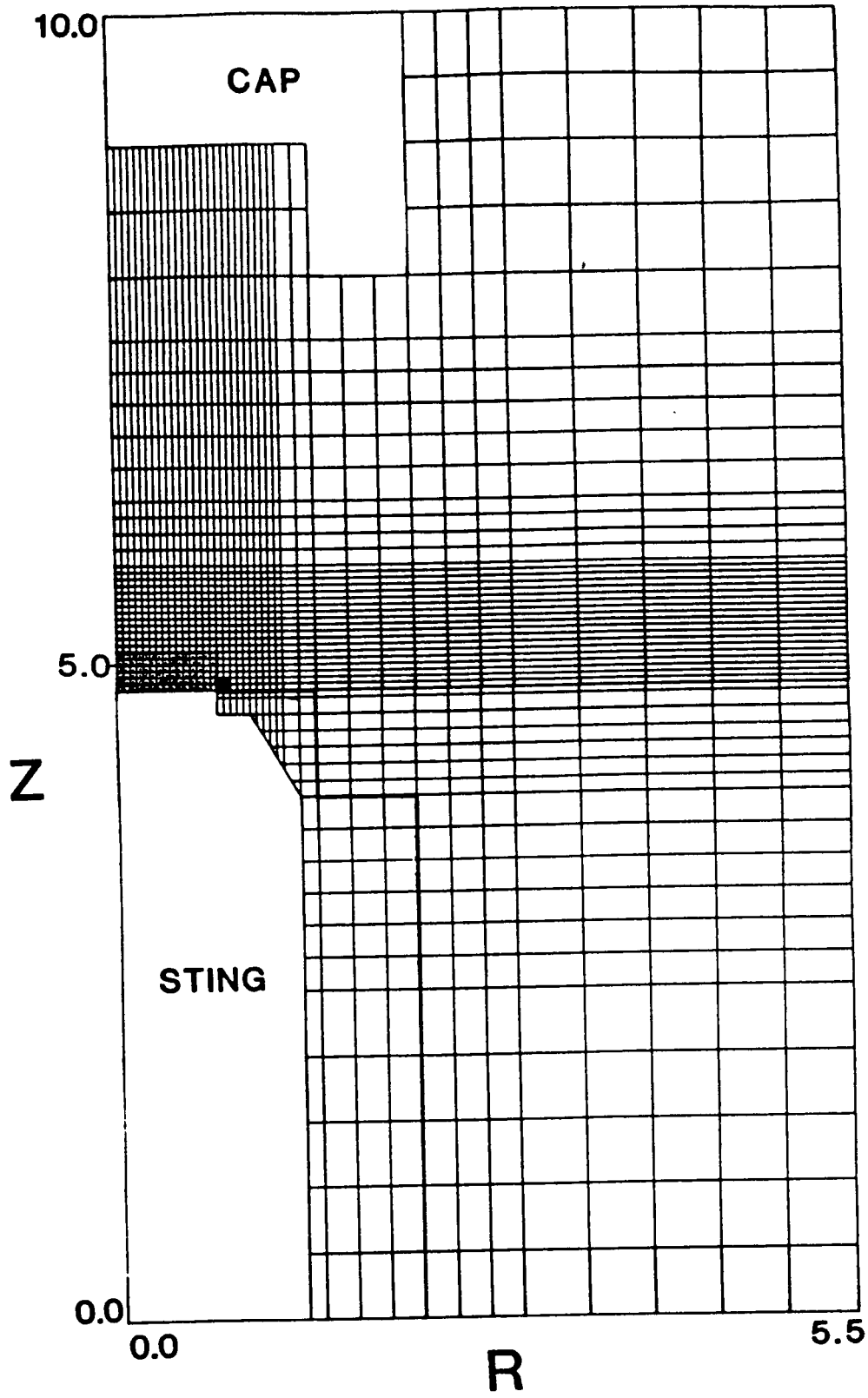

Figure 10. Mesh used for finite difference solution. Numbers are distances in cm.

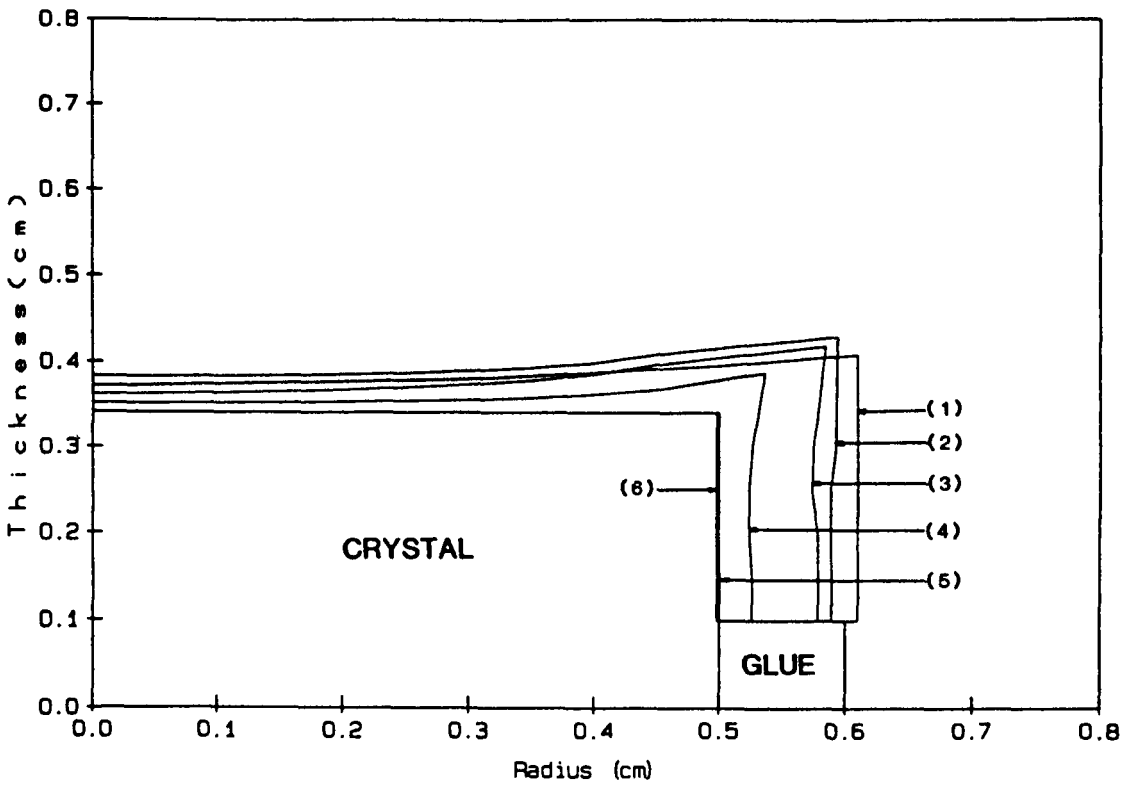

Figure 11. Comparison between the final shape of the crystal grown in Cell 3:

(1) Averaged from experimental values in Figure 4.

(2) Calculated using $D = 3 \times 10^{-5}$ cm^2/s.

(3) Calculated using $D = 2 \times 10^{-5}$ cm^2/s.

(4) Calculated using $D = 1 \times 10^{-5}$ cm^2/s.

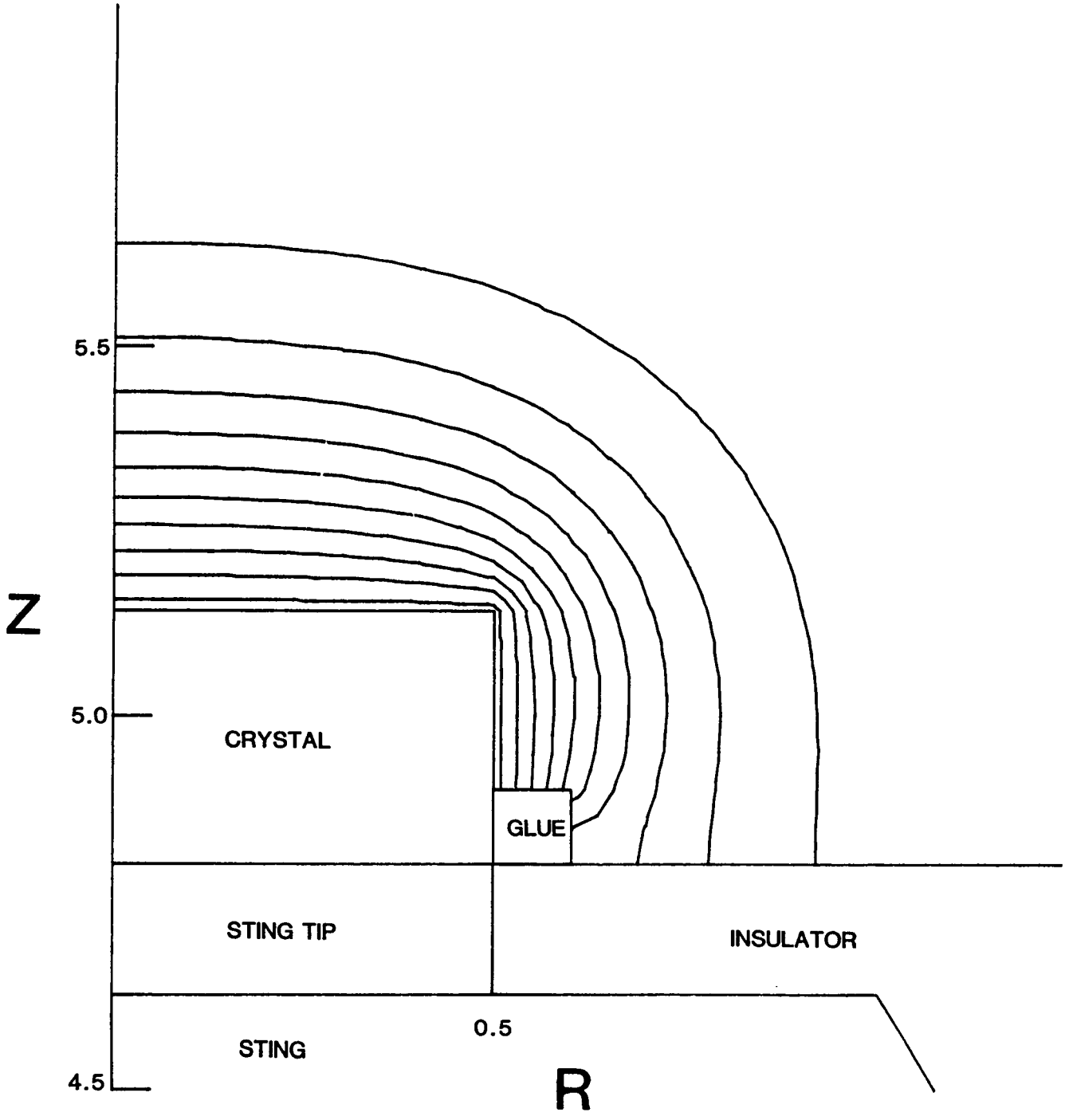

Figure 12. Isoconcentration lines for Cell 3 at end of isothermal dissolution period, 40.83 minutes after cap retraction, calculated using $D = 2 \times 10^{-5}$ cm^2/s. $T = 46$ C, concentration at crystal surface = 1.229 $mmol/cm^3$, original concentration of solution = 1.209 $mmol/cm^3$, change in concentration between lines = 0.002 $mmol/cm^3$.

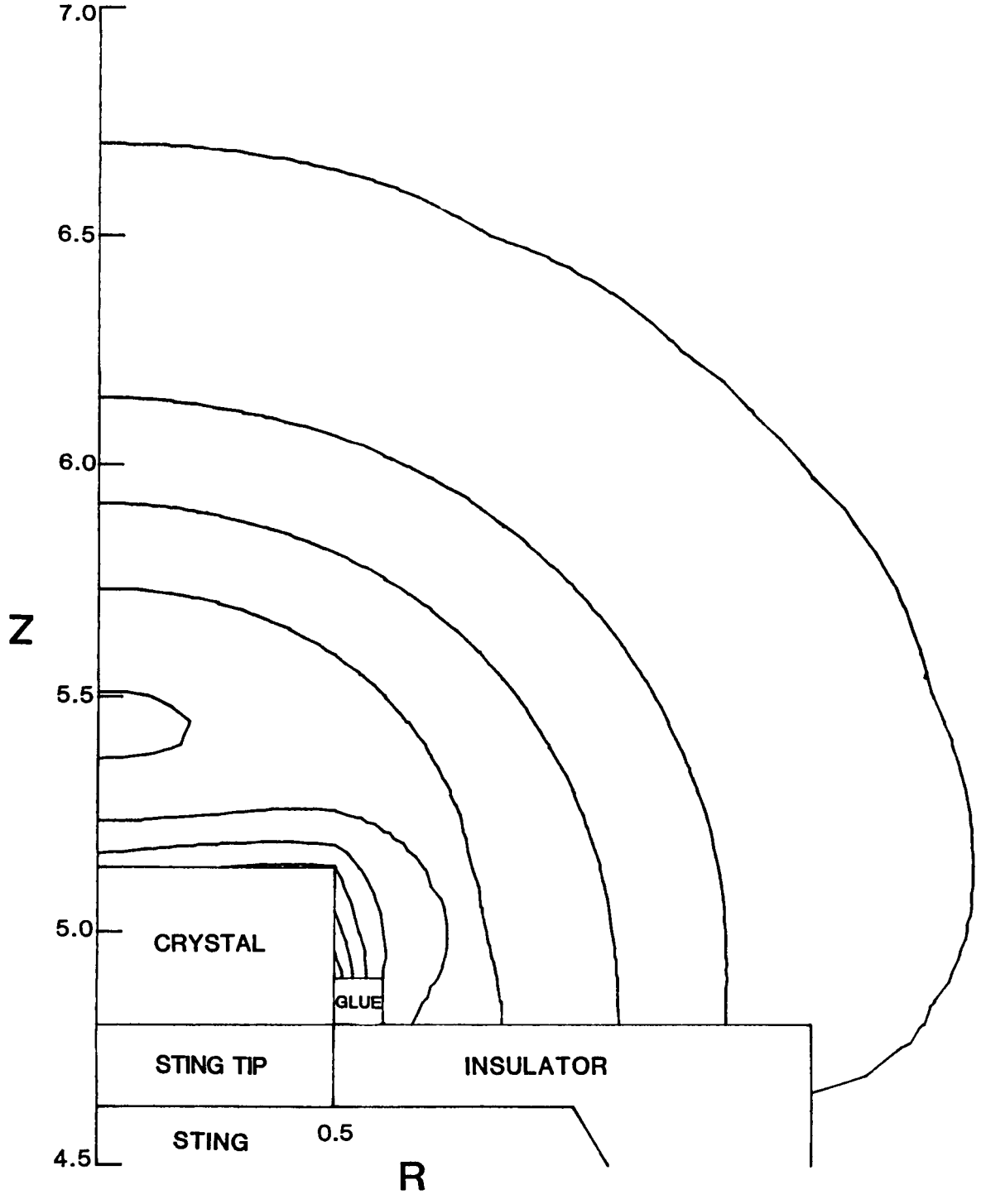

Figure 13. Computed isoconcentration lines for Cell 3 during linear cooldown period, 208.67 minutes after cap retraction. Change in concentration between lines = 0.001 mmol/cm^3. Maximum concentration at about Z = 5.4 cm, R = 0.

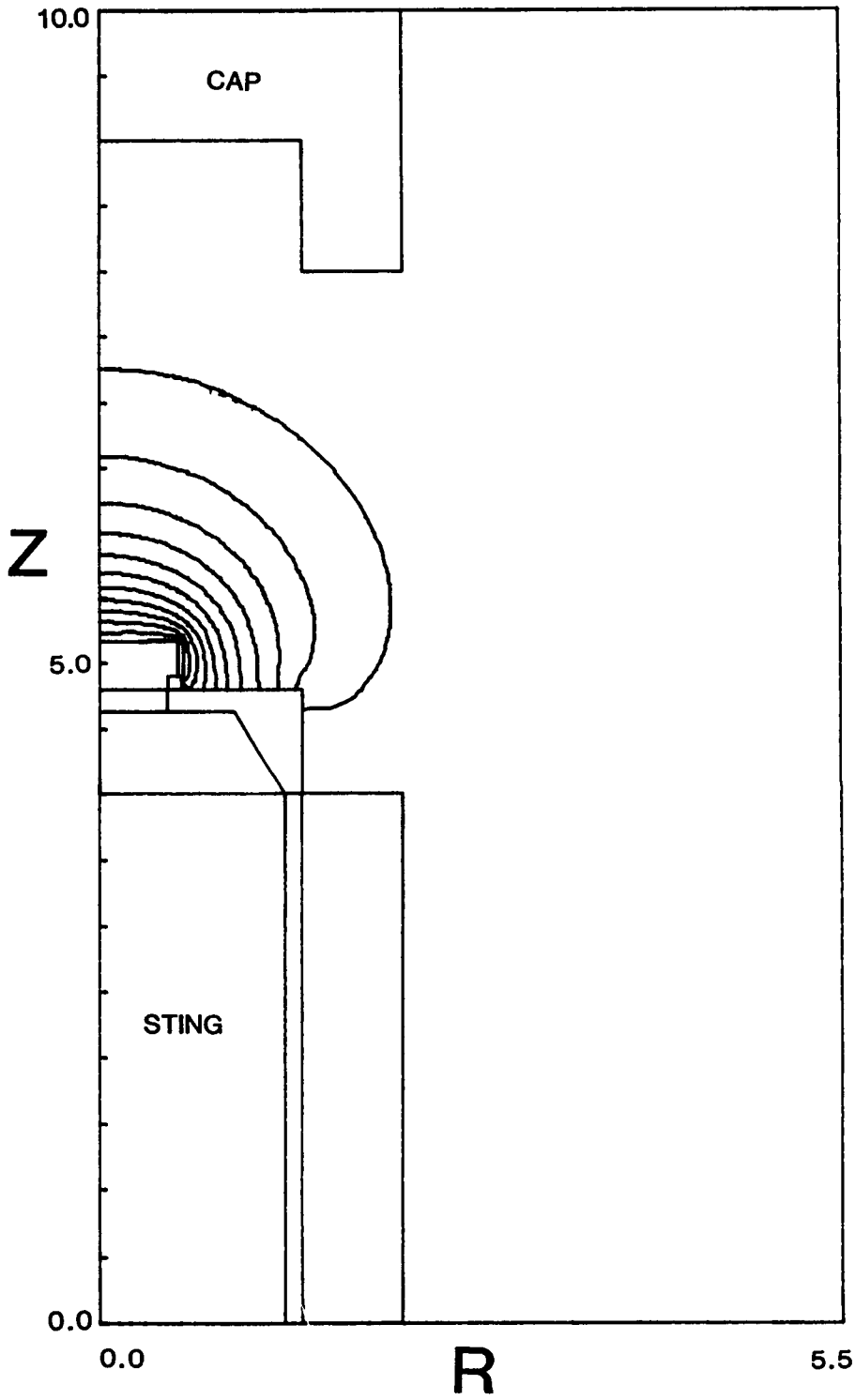

Figure 14. Computed isoconcentration lines for Cell 3 at end of run, 33.97 hours after cap retraction.

Change in concentration between lines = 0.005 mmol/cm^3.

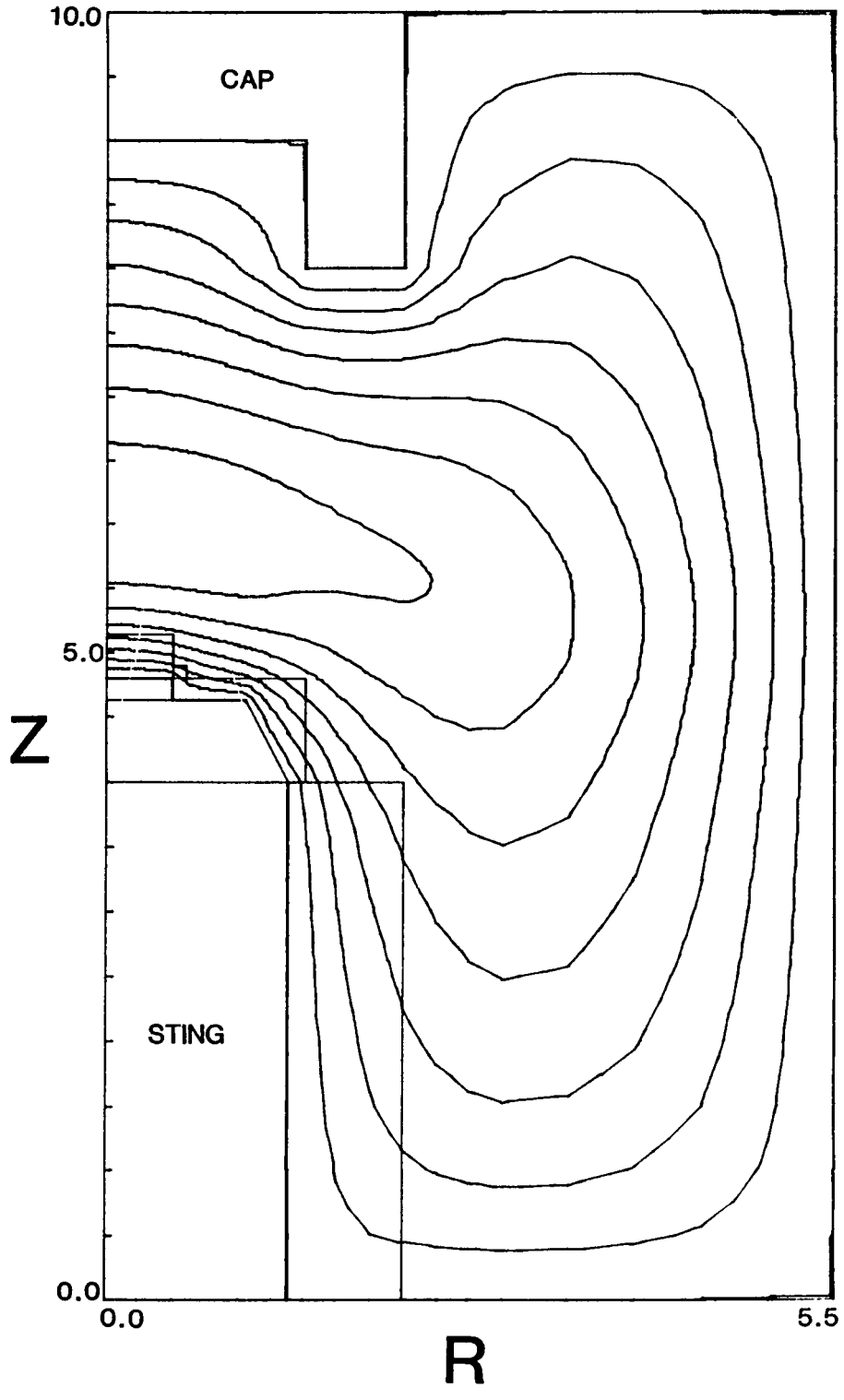

Figure 15. Isotherms for Cell 3 during linear cooldown period, 330.62 minutes after cap retraction. Wall temperature and sting temperature are 43.9 C.
Change in temperature between lines = 0.05 C.

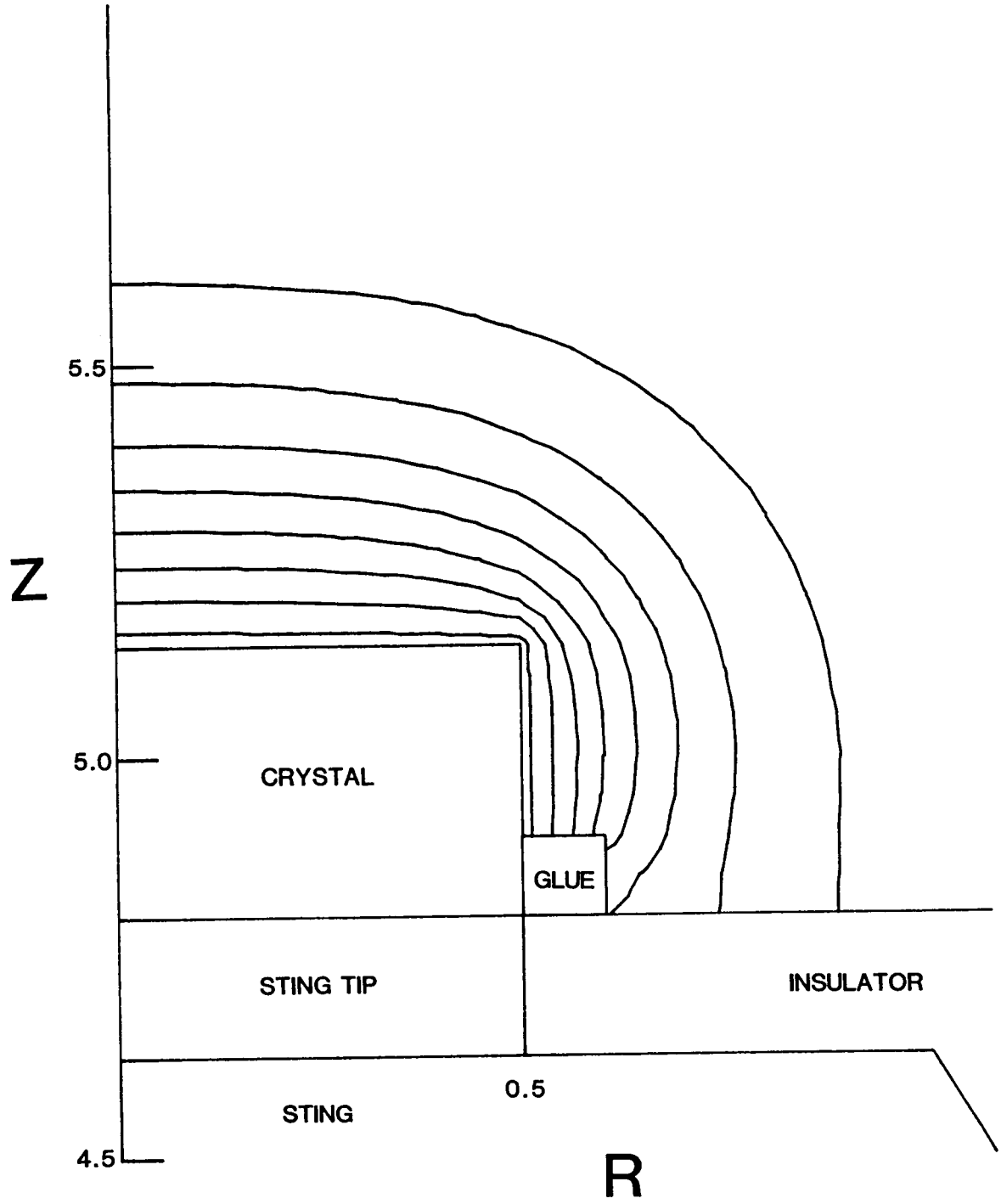

Figure 16. Computed lines of constant refractive index for Cell 3 at end of isothermal dissolution, 40.83 minutes after cap retraction. Refractive index of solution at top crystal surface is 1.38345.
Change in refractive index between lines = 0.0001.

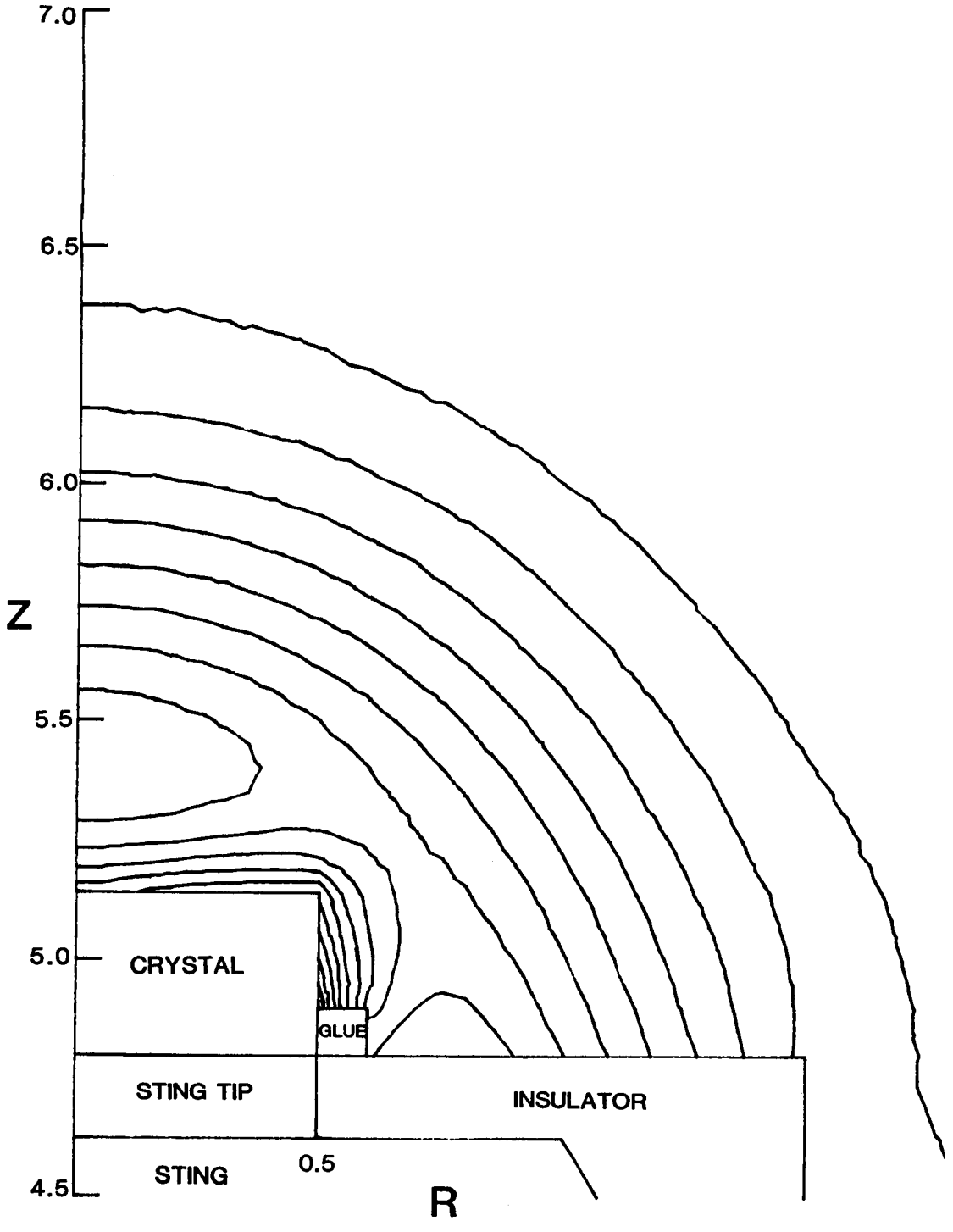

Figure 17. Computed lines of constant refractive index for Cell 3 in the linear cooldown period, 208.67 minures after cap retraction. Refractive index of solution at top crystal surface is 1.38286.
Change in refractive index between lines = 0.00002.

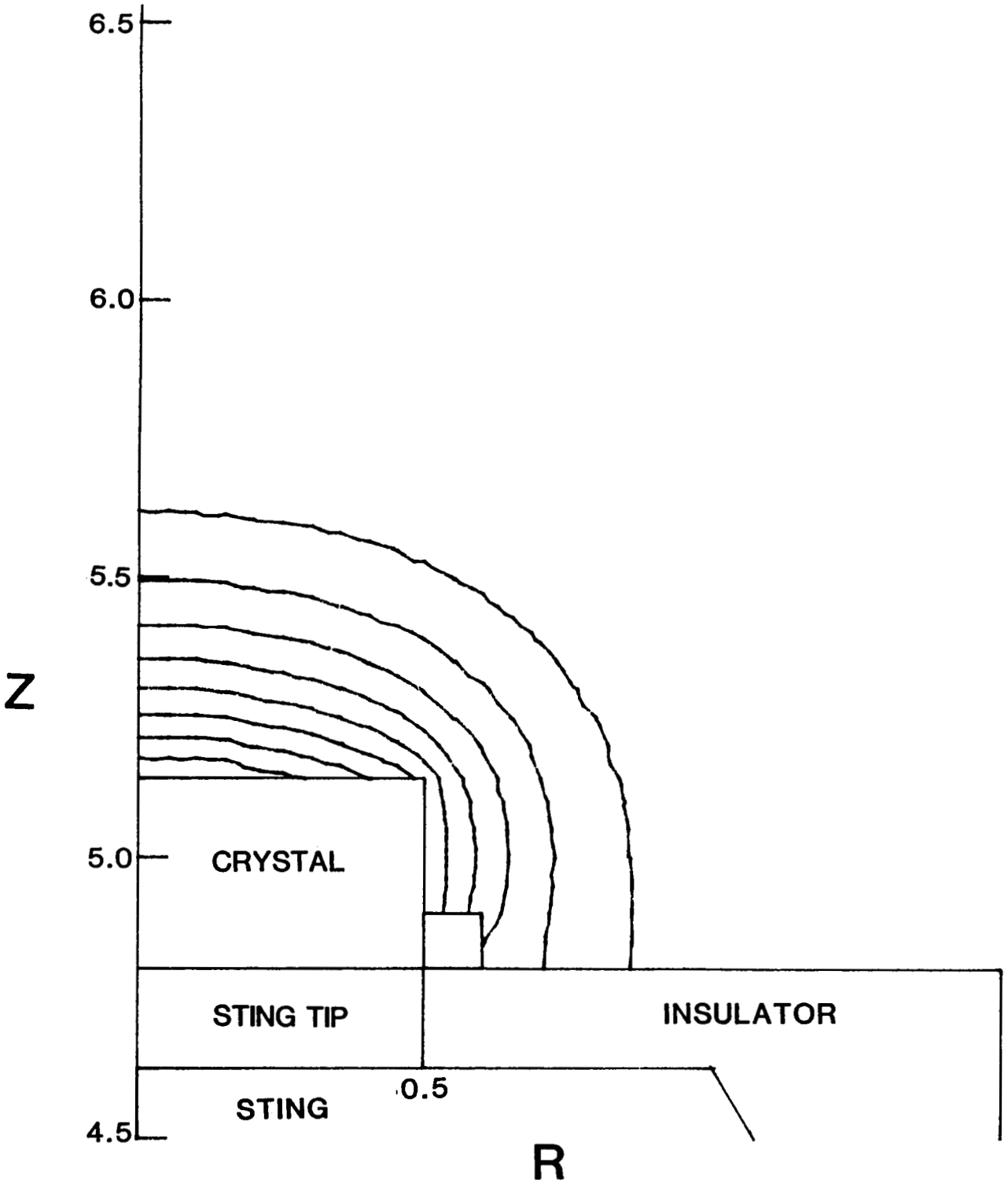

Figure 18. Computed interferogram for Cell 3 at the end of the isothermal dissolution period, 40.83 minutes after cap retraction. Compare with experimental interferogram in Figure 6.

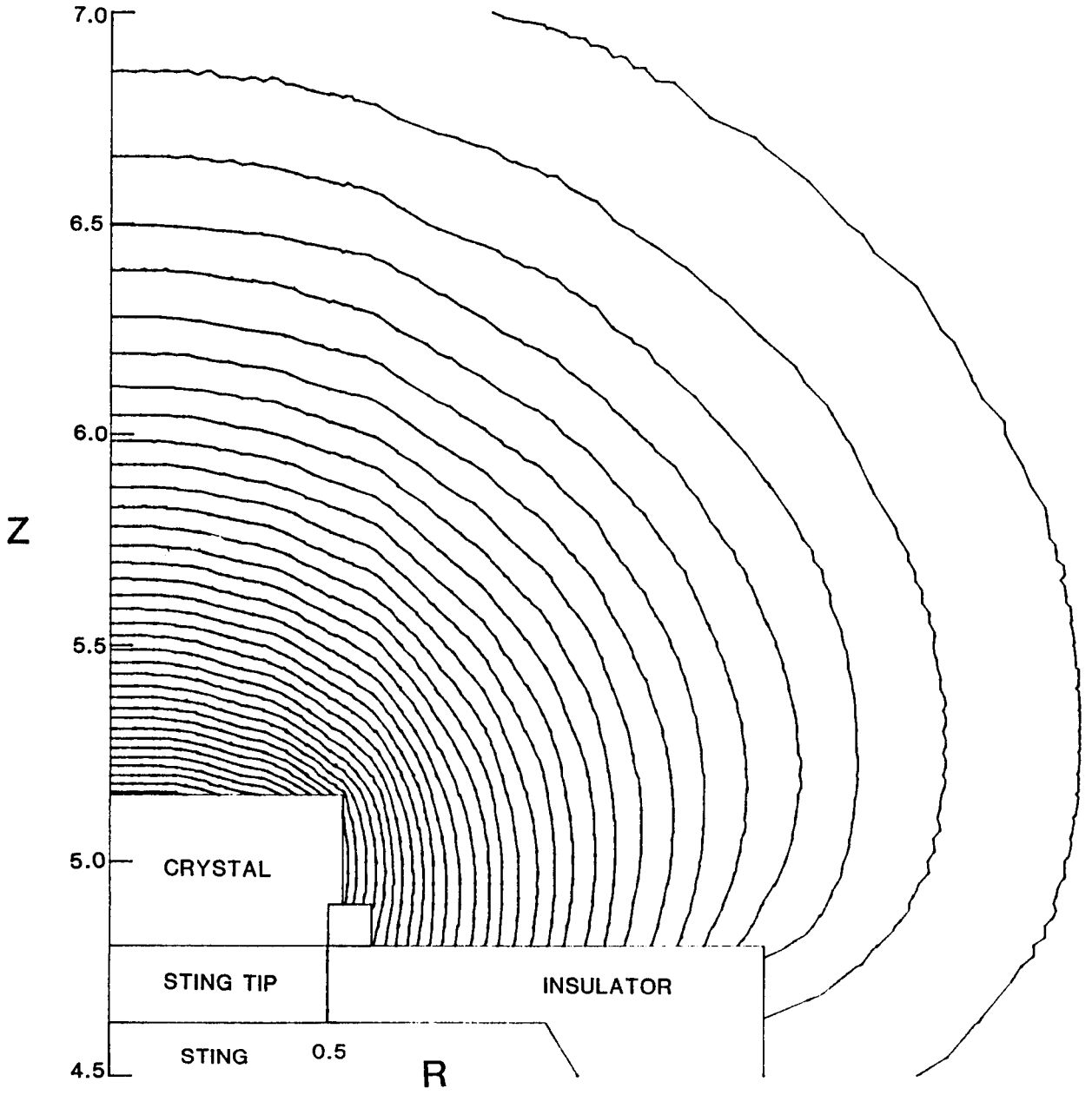

Figure 19. Computed interferogram for Cell 3 in the constant temperature period, 16.87 hours after cap retraction. Every other interference line was deleted for clarity. Compare with experimental interferogram in Figure 7.

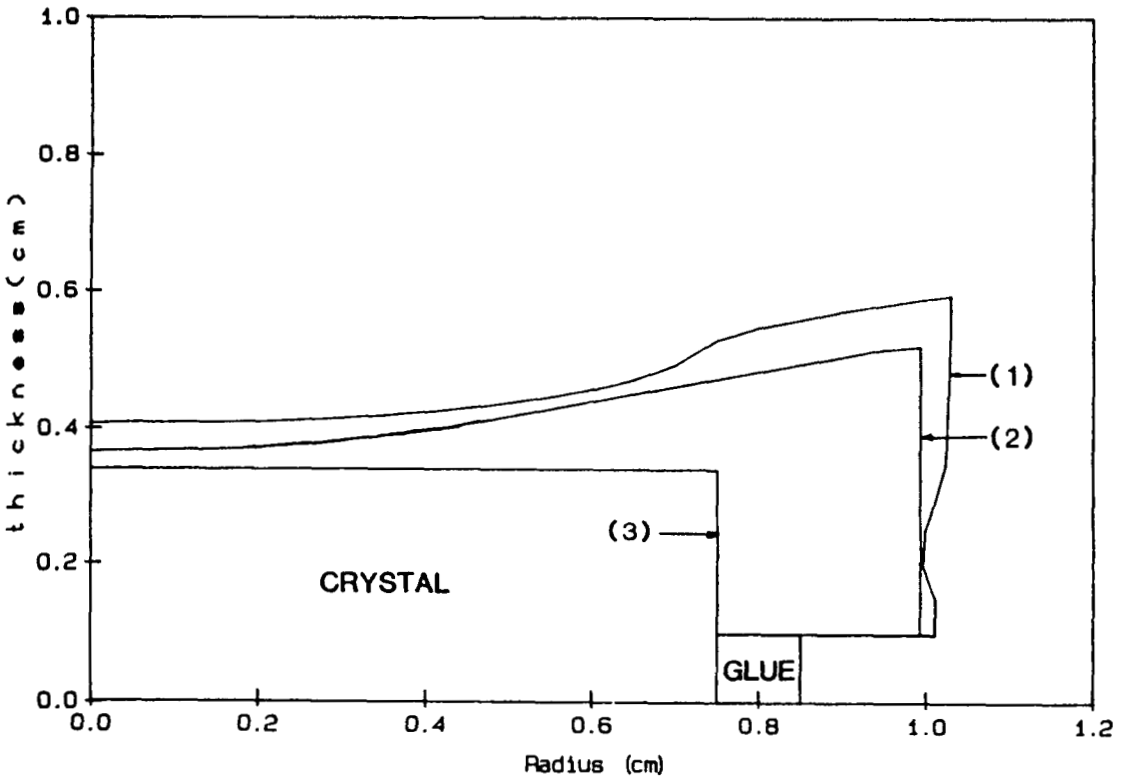

Figure 20. Comparison between experimental and computed crystal shape for Cell 2.

(1) Calculated using $D = 2 \times 10^{-5}$ cm^2/s.
(2) Averaged from experimental measurements.
(3) Original seed crystal.

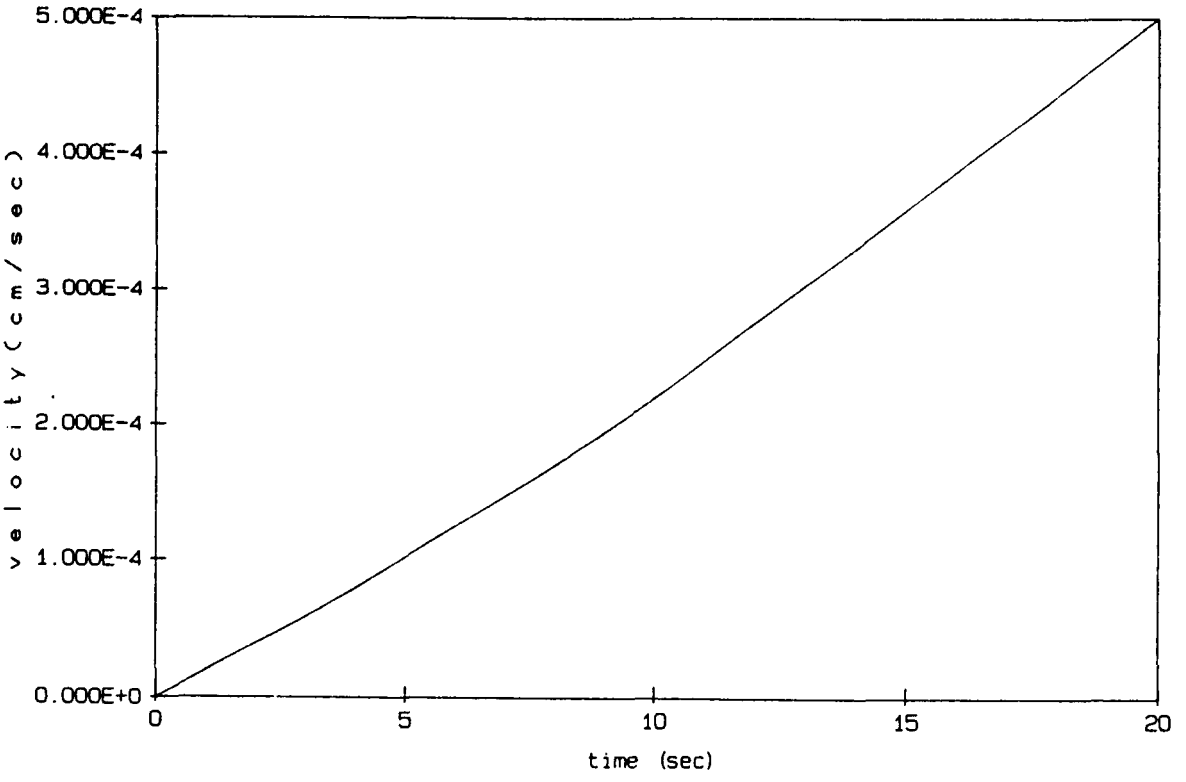

Figure 21. Maximum fluid velocity vs. time after turning 10^{-4} g acceleration (Gr = 14) on in Cell 2 after 46 hours of diffusion without convection.